Systematics of preequilibrium contributions in (n,p) reactions at 14 MeV

Gulzar Singh, H. S. Hans, T. S. Cheema, K. P. Singh,* D. C. Tayal,† and Jahan Singh‡
Department of Physics, Panjab University, Chandigarh, India

Sudip Ghosh
Saha Institute of Nuclear Physics, Calcutta, India
(Received 6 July 1993)

The existing up to date global data on angle integrated energy spectra (AIES) and energy integrated angular distributions (EIAD) of protons from (n,p) reactions at 14 MeV nominal neutron energy have been analyzed to develop systematics in relative preequilibrium contributions (RPC). The experimental estimates of RPC were obtained either from asymmetric components of the extrapolated EIAD or from the analysis of AIES, by comparison with equilibrium contributions obtained from the Hauser-Feshbach model. The experimentally obtained RPC have been compared with those expected from recent Feshbach-Kerman-Koonin theory as extended by Kalbach *et al.* as well as with theoretical predictions by Brown and Muirhead. The mass number systematics of RPC manifest shell and even-odd effects. The fraction of the precompound nucleus decays obtained from RPC, using the Blann-Griffin model, is constant and small for $A \geq 72$, and increases to about 1 for small A's. The analysis with the Kalbach model yields the dependence of the level density parameters a_1 and a_2 on A; also values of a_1 and a_2 manifest prominent structures near closed shell nuclei. The values of a_1 for compound nucleus are systematically higher than a_2, for the residual nuclei by an amount much larger than expected by usual A dependence, indicating excitation energy dependence of the single particle level density g. The excitation energy dependence of g when explored in the light of Rosenzweig's positive power law, with parameters n and k, reveals that for most cases $1.2 \leq n \leq 1.5$, with no systematic dependence of n on A, compared to reported theoretical values of $n \simeq 1.6$ by Rosenzweig, and $0.8 \leq k \leq 3.8$ with a trend of slow increase of k with A.

PACS number(s): 25.40.Kv, 24.60.Gv, 24.60.Dr

I. INTRODUCTION

A large amount of experimental data exists in the literature for the energy spectra and the angular distributions of the protons emitted from the (n,p) reactions at 14 MeV nominal neutron energy [1,2,3–37]. However, no overall systematics and uniform analysis of these data for the reaction mechanism has been reported so far. The available results for the reaction mechanism have many drawbacks. In their analysis, several workers [3,4] have not properly taken into account the (n,np) and (n,d) contributions. Some workers [5] have attempted to determine the relative preequilibrium contributions by taking the ratio of the differential cross sections at the forward and backward angles only.

With a view to develop the charge or mass systematics of the relative preequilibrium contributions, we analyzed the available global data [1–37] on the (n,p) reactions at 14 MeV, through the standard procedures as described in the subsequent sections.

For the earlier [1–27] data, the angular distributions for the energy range $E_p \geq 3+1$ MeV were obtained either directly from the literature or by integration of the angular distributions data available in the literature over different intermediate energy ranges. The preequilibrium contribution to the integrated cross section was determined by estimating the asymmetric part of the area graphically under the angular distribution curve. The contributions from the (n,np) reactions, when present over the pertinent proton energy range, were taken into account during the analysis [18,27] assuming these to proceed through the compound process. In general, we selected the angular distribution data of those workers only who had eliminated the (n,d) contributions. For other cases, the expected estimated positive bias from the (n,d) reactions to the relative preequilibrium contributions has been included in the errors.

Recently many workers [28–33] have measured the angle integrated energy spectra (AIES) with many targets and have compared them with multistage Hauser-Feshbach [38] and precompound models [39]. Also new EIAD measurements are available [34–37]. We have, therefore, used a different approach to extract the preequilibrium component from this data. As, for example, in a series of papers, Haight and co-workers [28–33] have measured the (n,p) reactions using V^{51}, ^{93}Nb, ^{89}Y, ^{90}Zr, $^{46-48}Ti$, $^{92-96}Mo$, $^{54,56}Fe$, $^{58,60}Ni$, and $^{63,65}Cu$ as targets and obtained the angle integrated energy spectra, which were compared with multistage Hauser-Feshbach calculations [38] as modified by Grimes and co-workers [29–33]. Intrinsically, these calculations correspond to the equilib-

*Presently at D.A.V. College, Chandigarh, India.
†Now at N.R.E.C. College, Khurja, U.P., India.
‡Presently at M. D. University, Rohtak, Haryana, India.

rium part of the reaction process and the difference between these calculations and the experimental data may be interpreted as the contribution from the nonequilibrium process. We have taken that as a semiempirical way of determining the contribution of the preequilibrium component of the reaction in these cases.

With so much data, there is a need for developing some systematics and their analysis, using the modern models of nuclear reactions [40–46] at these energies.

Apart from the MSC (multistep compound) and MSD (multistep-direct) calculations, from the Kalbach model [42–46], the results were, therefore, also compared with the predictions of Brown and Murihead [40], and the earlier version of the Blann-Griffin statistical model [41].

Finally, we have calculated, from our data, the parameters of the power law of Rosenzweig [47].

II. DATA ANALYSIS

A. Earlier data [1–27]

At high excitation energies involved in the present work, one expects the compound nucleus contribution to exhibit (on integration over a broad range of the exit channel energies) either an isotropic or smooth symmetric characteristics in angular distributions around the 90° angle in the center-of-mass system. The asymmetric portion of the angular distributions data, on the other hand, represents the major part of the preequilibrium mode. These distributions are, however, expected to develop isotropy towards the lower-energy side of the spectra [14]. To minimize this effect, as well as the (n,np) reaction contribution, we would have preferred to consider the angular distribution data for higher-energy protons only. However, due to the requirements of a broad range of the exit channel energies, and the desirability of maintaining an identical energy range for the development of the systematics of relative preequilibrium contributions, we have been constrained to analyze the angular distribution data integrated over a relatively wide proton energy range defined by $E_p \geq 3 + 1$ MeV. The angular distributions in all cases peaked in the forward direction. For some cases either the values continuously go on decreasing as for ^{27}Al and ^{103}Rh or curve upward for some cases like ^{40}Ca. For all the categories of angular distributions, we draw smooth symmetrical curves around 90° passing through the most backward angles to represent the area of the isotropic (or symmetrical) portion of the angular distribution as A_s: and the forward asymmetrical part as A_{as}. The relative preequilibrium contributions D_1 to the integrated (n,p) cross section over the common energy range is then defined as

$$D_1 = \frac{A_{as}}{A_{as} + A_s} . \tag{1a}$$

In some cases, angular distribution data carry the significant contribution from (n,np) reactions. In such cases we have applied the necessary correction by a similar procedure as followed by Alvar [27] and Hassler and Peck [18].

Assuming that the (n,np) reaction proceeds entirely through the compound nucleus formation, an isotropic distribution for the (n,np) contribution was drawn and substracted from the experimental angular distribution curves before calculating the relative preequilibrium contribution. The corrected contribution has been denoted by D_{1c}.

B. Recent data [28–37]

Using the procedure mentioned earlier, we substracted the integral area under the theoretical curve calculated

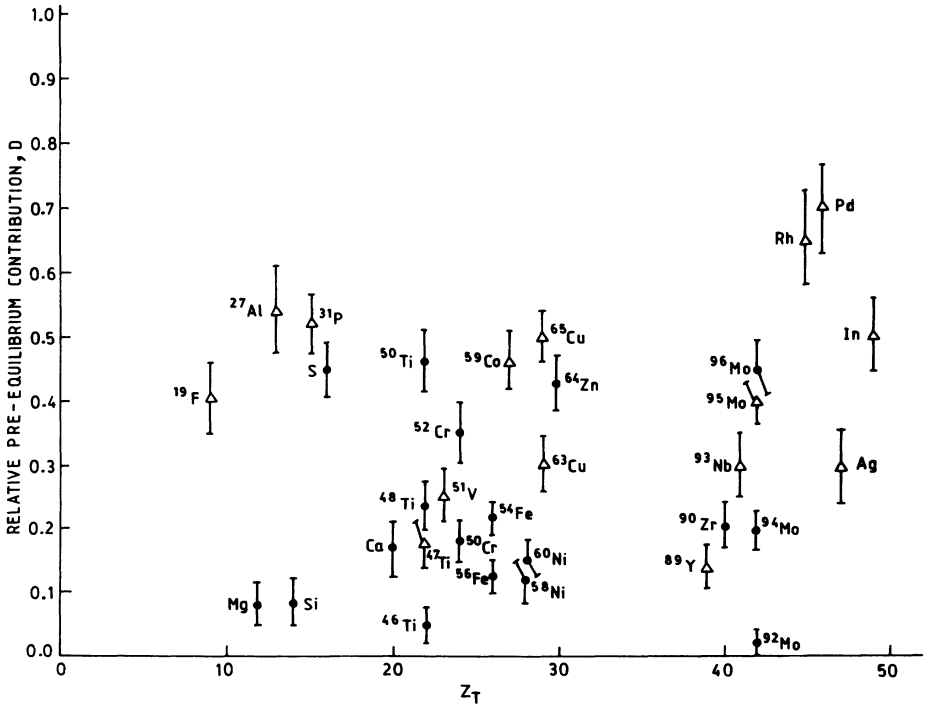

FIG. 1. Experimental relative preequilibrium contributions to the integrated (n,p) cross sections (D) versus target charge number Z_T. • represent even and △ represent odd nuclei.

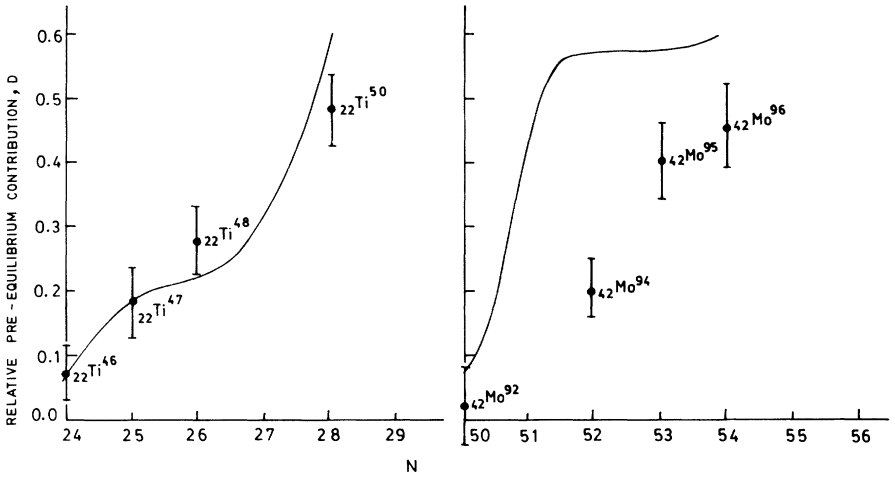

FIG. 2. Experimental value of D as a function of N (neutron member) for various isotopes of Mo and Ti and theoretical curves from Kalbach model.

on the basis of the multistep Hauser-Feshbach model [38] from the total area under the experimental points in the various energy spectra of protons (Refs. [29–33]) and defined D_3 as

$$D_3 = \frac{N_T(\text{Expt}) - N(\text{Theor})}{N_T(\text{Expt})} , \tag{1b}$$

where N_T(Expt) corresponds to the total area in the angle integrated proton emission spectra from the possible measured low-energy end of protons above the (n, np) portion to the highest-energy end of the measured spectrum. The quantity N_T(Theor) similarly corresponds to the total area under the theoretical curves for the equilibrium part of the spectrum in the same proton energy range. The errors in the value of D_3 are obtained from the quoted errors in the experimentally measured points. The results for D_{1c} as well as D_3 have been plotted in Fig. 1 versus the charge number Z_T of the target nuclei, denoted as D. The values of D are summarized as $D_{(\text{Expt})}$in Table II.

However, for In and Ag, where the experimental angular distributions integrated above 6 MeV are available and for other recent data [35–37], we have followed the same procedure, as previously mentioned for the earlier data corresponding to D_1, and have plotted them in Fig. 1 along with the rest of the recent values of direct contribution.

In Fig. 2 we have plotted the values of D for different isotopes of Mo and Ti as a function of the neutron number as obtained form the data by Grimes and co-workers [29–33] and Rebamsky and Gmuca [34] along with theoretical curve from Kalbach model [46]. It is interesting to note the increase of D with the neutron number in both these cases.

III. THEORETICAL COMPARISONS

A. Blann-Griffin model [41]

According to the Blann-Griffin statistical model [41], the probability $W_c(E)dE$ of decay per unit time of a compound nucleus at excitation energy E_c and characterized by the level density $\rho(E_c)$, through the proton channels having energy between E and $E + dE$ and reduced mass m and to the residual nucleus at the excitation energy E_R, is given by the expression

$$W_c(E)dE = F_{ac}\frac{\rho(E_R)}{\rho(E_c)}\left[1 + \left(\frac{E_R}{E_c}\right)^2 + \left(\frac{E_c}{E_R}\right)^2\right]dE . \tag{2}$$

The probability for the preequilibrium decays $W_p(E)dE$ into these channels is, however, expressed [41] as

$$W_p(E)dE = F_{ac}\left(\frac{E_c}{E_R^2 g}\right)\sum_{\substack{n \geq 3 \\ \Delta_n = 2}}^{\bar{n}}\left(\frac{E_R}{E_c}\right)^n (n^2 - n)dE \tag{3}$$

with the factor

$$F_{ac} = \frac{2mE\sigma(E)}{\pi^2\hbar^3} . \tag{4}$$

Cross sections $\sigma(E)$ for the observed protons on the residual nuclei were obtained from Table 4.1, page 352 of Ref. [48] with the nuclear radius parameters $r_0 = 1.3$ fm. The quantity $\bar{n}$ is defined through the average single particle level density g of the compound nucleus, which can be obtained from Ref. [41] as

$$\bar{n} = (gE_c)^{1/2} \tag{5}$$

and level density $\rho(E_c)$ as

$$\rho(E_c) = \text{Const} \times E_c^{-1}\exp[2(gE_c)^{1/2}] . \tag{6}$$

Expressions (2) and (3) were integrated by us over the appropriate range of E_R defined by $E \geq 2 - 5$ MeV to the maximum possible value defined by the Q values for the (n, p) reactions. According to this model, the total emission probability for channel energy E is given by

$$W(E) = \alpha_p W_p(E) + (1 - \alpha_p) W_c(E) \ , \qquad (7)$$

where α_p is the fraction of precompound decays into continuum channels. To compute the parameter α_p the fraction of the precompound decays and, therefore, $\alpha_c = 1 - \alpha_p$, the following expression for D was used, where D's are the experimental values of the preequilibrium contributions defined in Sec. II, obtained from earlier data as well as the recent data:

$$D = \frac{\alpha_p \int W_p(E) dE}{\alpha_p \int W_p(E) dE + (1 - \alpha_p) \int W_c(E) dE} \ . \qquad (8)$$

The values of α_p obtained from Eq. (8) are listed in Table II; α_c are also plotted versus target mass number A in Fig. 3, along with earlier available results from (p, n) reactions at about 18 MeV proton energy [49]. These data sum up the global results on α_c. We have also plotted in the inset of the same figure the values of α_p versus $1/R$, where R is the radius of the target nucleus, taking $R = 1.2 \times 10^{-}13A^{1/3}$ cm.

The present α_c values as well as the values reported in literature for the (p, n) reactions at 18 MeV protons [49], as apparent from Fig. 3, follow an overall trend of the sharp rise with A up to $A \simeq 72$ beyond which α_c assumes nearly a constant value of unity for all targets.

The experimental points for α_p when plotted against $1/R$ seem to follow two distinct smooth curves, which may be expressed as

$$\alpha_p \simeq \lambda \left(\frac{1}{R} - \frac{1}{R_0} \right) \quad \text{for } R \leq R_0 \ , \qquad (9a)$$

where $\lambda \simeq 5.3 \times 10^{-13}$ cm and $R_0 \simeq 5 \times 10^{-13}$ cm (this value of R_0 corresponds to $A = 72$) and

$$\alpha_p \ll 0.1 \quad \text{for } R \geq R_0 \ . \qquad (9b)$$

One may interpret qualitatively and physically the above relations as follows: The parameter α_p seems to be constant and very small ($\alpha_p \ll 0.1$) for heavier nuclei ($R \geq R_0$); because in these cases the mean free path of 14 MeV neutrons may be smaller or of the same order as the radius of the nucleus; hence the probability of interaction with the other nucleons in the nuclear volume is expected to be comparatively large and, therefore, the small probability of the decay of a precompound channel to continuum may reproduce the experimental preequilibrium contribution as the model predicts. For smaller nuclei, one seems to require a large and A-dependent α_p to explain the experimental data, showing that perhaps surface plays a bigger role now and the emitted particle reaches the continuum state with a larger probability than expected from the model.

B. Kalbach model [42–46]

The preequilibrium reaction mechanism is conveniently understood in terms of the exciton model. The target-projectile composite nucleus is assumed to reach compound nucleus equilibrium through a cascade of two-body interactions. Each stage of the cascade is characterized by the number of excited particles p and holes h, called excitons. Preequilibrium emissions can take

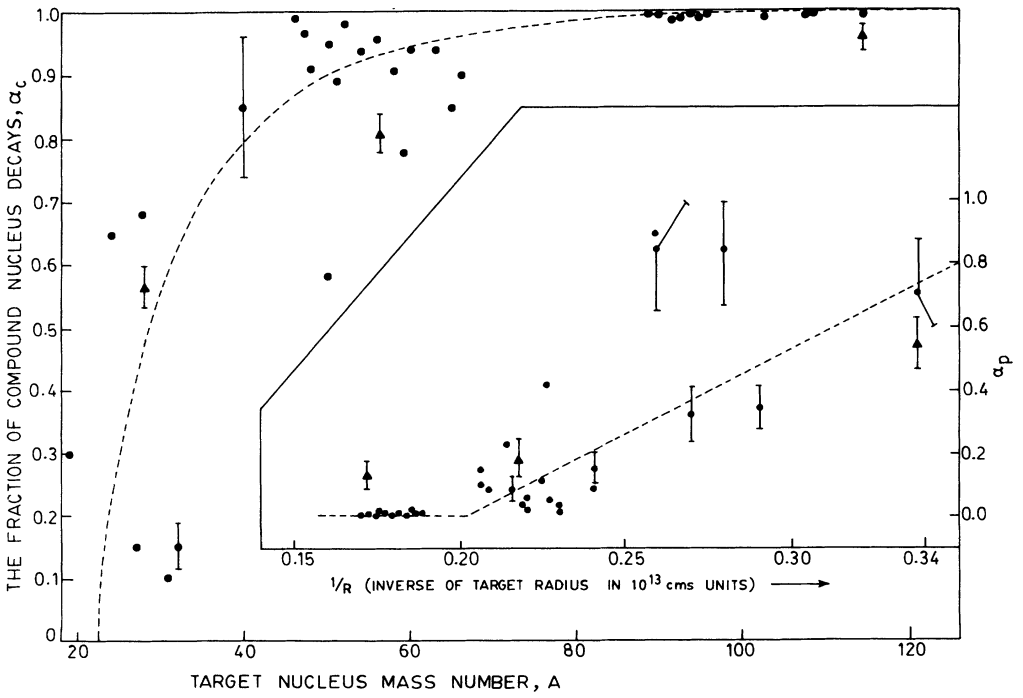

FIG. 3. The fraction of compound decays α_c versus the target nucleus mass number A. The circular dots (•) represent the present results, while triangular points (▲) show the only available previous data from (p, n) reactions [49] at $E_p = 18$ MeV. The inset displays the variation of fraction α_p of the preequilibrium decays with the inverse of the target nucleus R, with $R = 1.2A^{1/3} \times 10\,\text{cm}^{-13}$. The errors on various points as indicated in some cases, are expected to be around 25–30%.

place from any stage of the cascade. There are several versions of the exciton models [39]. For the present work we use the semiclassical model of Kalbach [42–46], which includes contributions from the statistical multistep-direct (MSD) and statistical multistep compound (MSC) processes of the Feshbach-Kerman-Koonin quantum-mechanical theory of preequilibrium reactions [42].

In the MSD process, at least one of the excited particles is in the continuum of states at each stage of the binary cascade. In the MSC process all the particle excitons are bound during the relaxation process and emissions take place through statistical fluctuations. The MSD and MSC components of the preequilibrium spectra are distinguished by their angular distributions. The MSD emissions are forward peaked while MSC emissions have an angular distribution symmetric about the 90° center-of-mass angle as in the case of purely compound nucleus emissions. The difference between MSD and compound nucleus emissions lies in the ejectile energy. The MSD ejectile carries more energy since the number of excited degrees of freedom is less than when compound nucleus equilibrium is reached.

The energy spectra of the preequilibrium ejectile is given by

$$\sigma_{\rm pre}(E) = \sigma_{\rm MSD}(E) + \sigma_{\rm MSC}(E) \ , \tag{10}$$

where $\sigma_{\rm pre}(E)$ and $\sigma_{\rm MSD}(E)$ are evaluated from the expressions

$$\sigma_{\rm pre}(E) = \sigma_{\rm abs} \sum_{p=p_0}^{\bar{p}} S_u(p,h) T_u(p,h) \lambda_c^{(u)}(p,h,E) \tag{11}$$

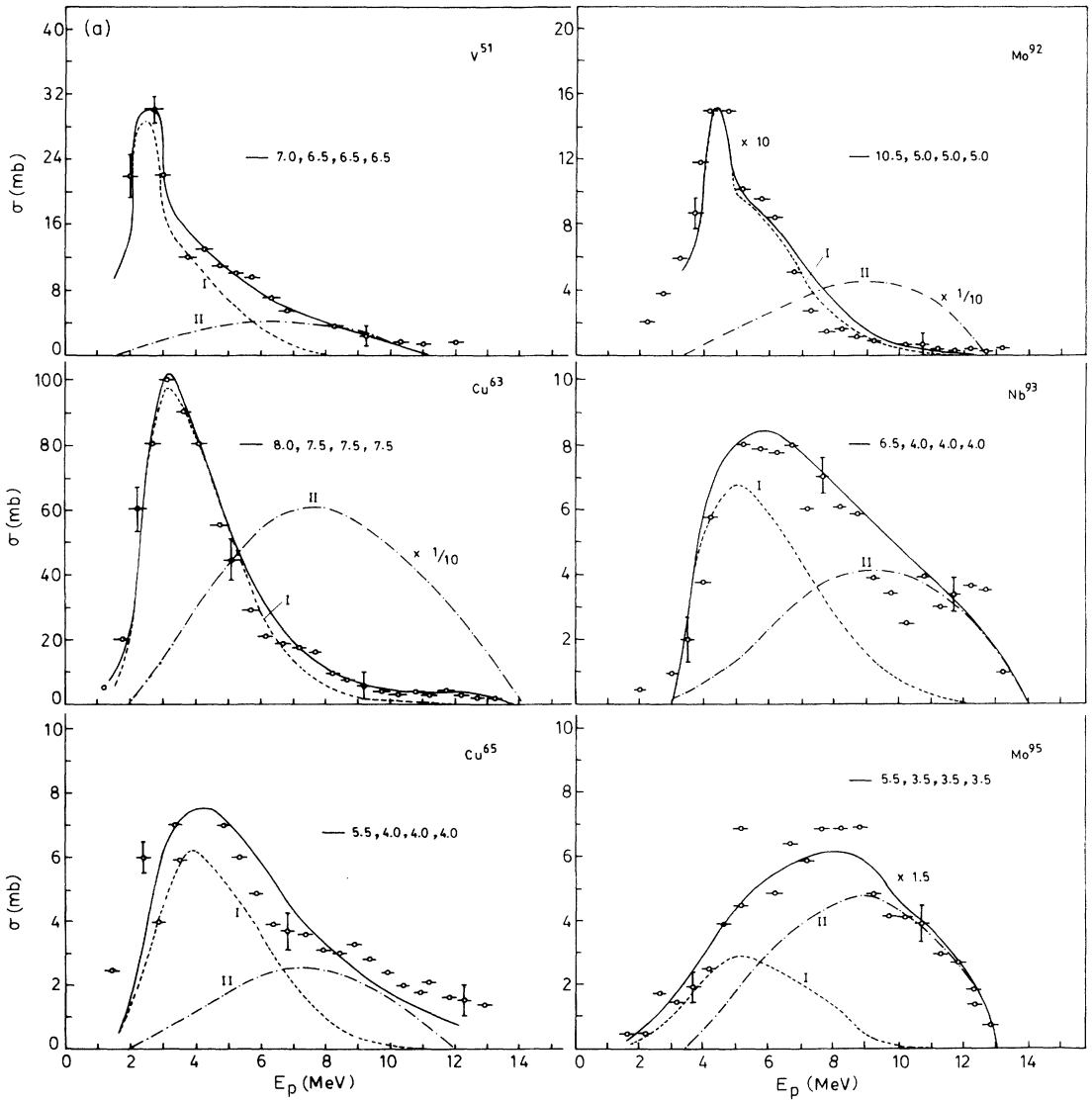

FIG. 4. (a) Typical experimental data on energy spectra and theoretical fits, with best-fit (Kalbach model) values of g's as shown (g_c, g_n, g_p, g_α). The curve marked as I(- - - -) in each case represents compound contribution, while that marked as II(·····) shows preequilibrium contribution. (b) Typical experimental angular distributions and the comparison with theoretical fits with values of g's as shown (g_c, g_n, g_p, g_α) (Kalbach model).

and

$$\sigma_{\mathrm{MSD}}(E) = \sigma_{\mathrm{abs}} \sum_{p=p_0}^{\bar{p}} S_d(p,h) T u(p,h) \lambda_c^{(u)}(p,h,E) \ . \quad (12)$$

σ_{abs} is the absorption cross section of the projectile on the target, p_0 is the number of particles excited in the first stage of the binary cascade, and $\bar{p}$ is the number of excited particles in the equilibrated compound nucleus. $S_u(p,h)$ is the probability of reaching a configuration with p excited particles and h holes with at least one excited particle in an unbound state. $S_d(p,h)$ is the probability of reaching the same (p,h) configuration with an excited particle in an unbound state with the additional constraint that each of the previous configurations from which the (p,h) configuration has evolved had at least one particle in the continuum. $T_u(p,h)$ is the mean life of the (p,h) configuration. $\lambda_c^{(u)}(p,h,E)$ is the emission rate of the ejectile with energy E from the (p,h) configuration.

$$\lambda_c^{(u)}(p,h,E) \propto \frac{\rho(p-A_b,h,U)}{\rho^{(u)}(p,h,E_c)} \ , \quad (13)$$

where $\rho^{(u)}(p,h,E_c)$ is the partial density of unbound states in the (p,h) configuration of the composite nucleus having excitation energy E_c, and $\rho(p-A_b,h,U)$ is the partial density of states for the residual nucleus at excitation energy U in the $(p-A_b,h)$ configuration with A_b the number of nucleons in the ejectile. Derivations and details of evaluation of $S_u(p,h)$, $S_d(p,h)$, $T_u(p,h)$, and $\lambda_g^{(u)}(p,h,E)$ are given in the Refs. [43,44]. With $\sigma_{\mathrm{pre}}(E)$ and $\sigma_{\mathrm{MSD}}(E)$ evaluated from Eqs. (11) and (12), $\sigma_{\mathrm{MSC}}(E)$ is obtained form Eq. (10). Then

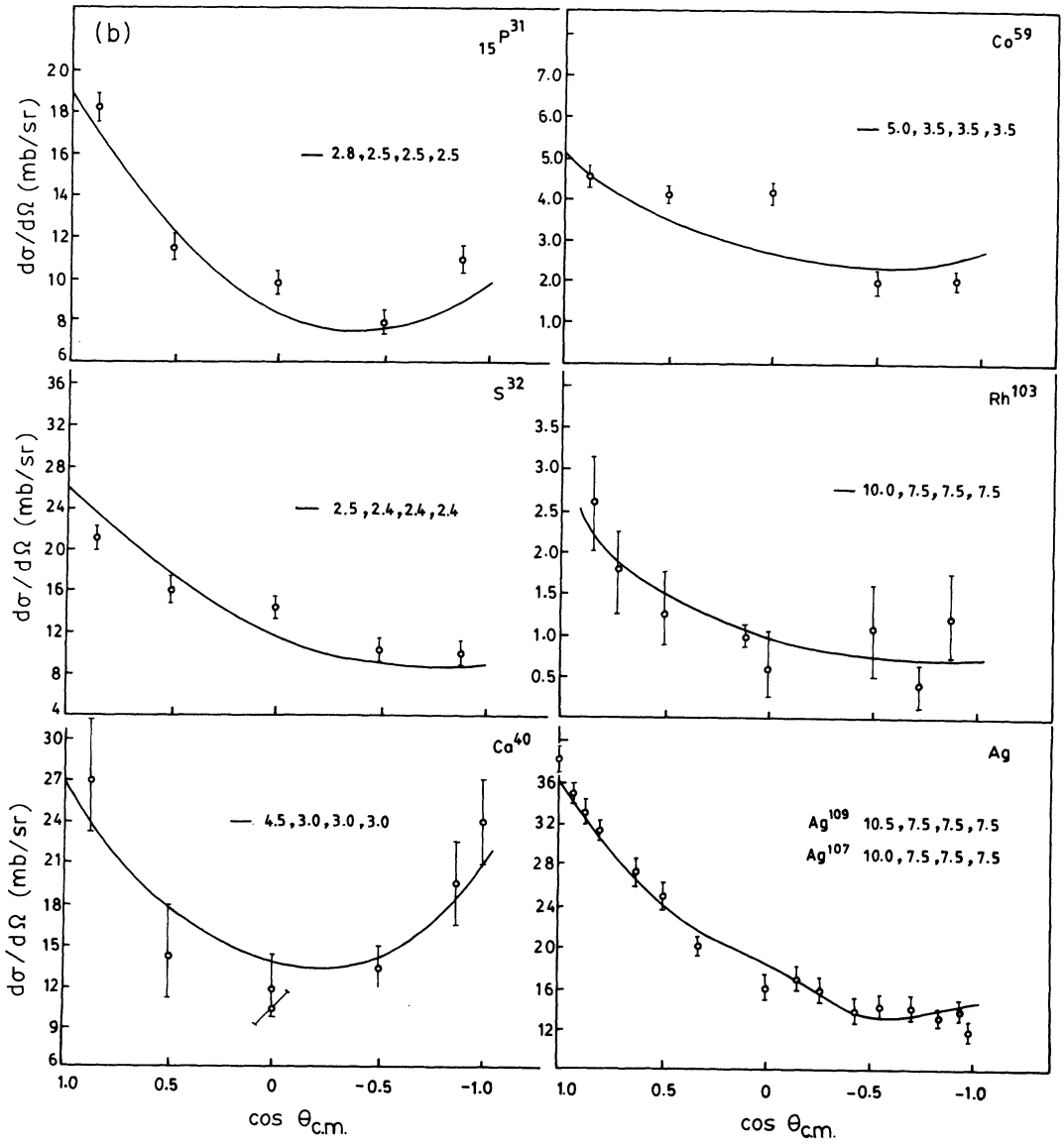

FIG. 4. (*Continued*).

$$\sigma_{\text{comp}} = \sigma_{\text{eV}} + \sigma_{\text{MSC}} , \tag{14}$$

where σ_{eV} has been obtained from Weisskopf-Ewing calculations [51].

The Kalbach model also includes some other classes of direct reactions not included in MSD. These are nucleon transfer and nucleon knockout. These are evaluated semiempirically as discussed elsewhere [50]. However, our calculations show that these processes do not contribute to the (n,p) channel.

The theoretical value of the fraction of the preequilibrium contribution $D_{\text{Th}-1}$ is then given by

$$D_{\text{Th}-1} = \frac{\int \sigma_{\text{MSD}}(E)}{\int \sigma_{\text{MSD}}(E) + \int \sigma_{\text{comp}}(E)dE} . \tag{15}$$

The computer code PRECO-D2 [46] has been used to evaluate $\sigma_{\text{pre}}(E)$, $\sigma_{\text{MSD}}(E)$, and $\sigma_{\text{comp}}(E)$ as described in Ref. [50]. The code also calculates the angular distributions for the preequilibrium and compound nuclear components of the ejectile spectra from the phenomenological Kalbach-Mann systematics [44]. This model has been used earlier [50] for obtaining the neutron spectra form alpha incident particles at 40–60 MeV.

The code needs the following input parameters: σ_{abs} of Eqs. (11) and (12) and the single-particle level densities g_R and g_c of the residual nucleus and the composite nucleus, respectively. g_R and g_c are needed to evaluate $\rho(p - A_b, h, U)$ and $\rho^{(u)}(p, h, E_c)$ of Eq. (13). PRECO-D2 calculates σ_{abs} using the semiempirical approximation of Chatterjee, Murty, and Gupta [52]. We treat σ_{abs} in Eqs. (11) and (12) as a scaling factor and obtain a normalized value of σ_{abs} by comparing the theoretical values of the total (n,p) cross sections calculated with the semiempirical expression of Ref. [52], with the experimental values of total (n,p) cross sections obtained from angular distribution or energy spectra. These normalized values of σ_{abs} are given in Table II. The single-particle level densities g_R and g_c were varied to obtain good fits with all the experimental data, keeping $g_R = g_p = g_\alpha$, where g_p, g_n, and g_α correspond to proton, neutron, and alpha emission. Values of the corresponding level density parameters $a_1 = \frac{\pi^2 g_c}{6}$ and $a_2 = \frac{\pi^2 g_R}{6}$ are given in Table I. The initial configuration of the first two-body interaction was taken as $p_0 = 2$ and $h = 1$. For the constant matrix element of the two-body interaction rate [42–46], we chose the default option of 135 MeV.

Comparison of the calculated and experimental energy integrated angular distribution ($E_p \geq 3$ MeV) and angle integrated energy spectra are shown in Figs. 4(a) and 4(b). For natural targets, the theoretical values were obtained for each naturally occurring isotope and their sum taken in proportion to their natural abundances. In each case, we searched and found a set of σ_{abs}, g_c, and g_R, which reproduce the shapes of energy spectra and angular distributions quite well, as shown for some typical cases in Figs. 4(a) and 4(b), and also reproduce the experimental value of relative preequilibrium contributions (RPC) to a large extent. The values of a_1 and a_2, obtained from best fits of g_c and g_R are given in Table I and plotted in Fig. 5 against the target mass number A, and the values of σ_{abs} are listed in Table II, which also contains $D_{\text{Th-1}}$ from Eq. (15). All the cases of energy spectra and angular distributions had, in general, a similar quality of fits as given in Fig. 4. The ratio

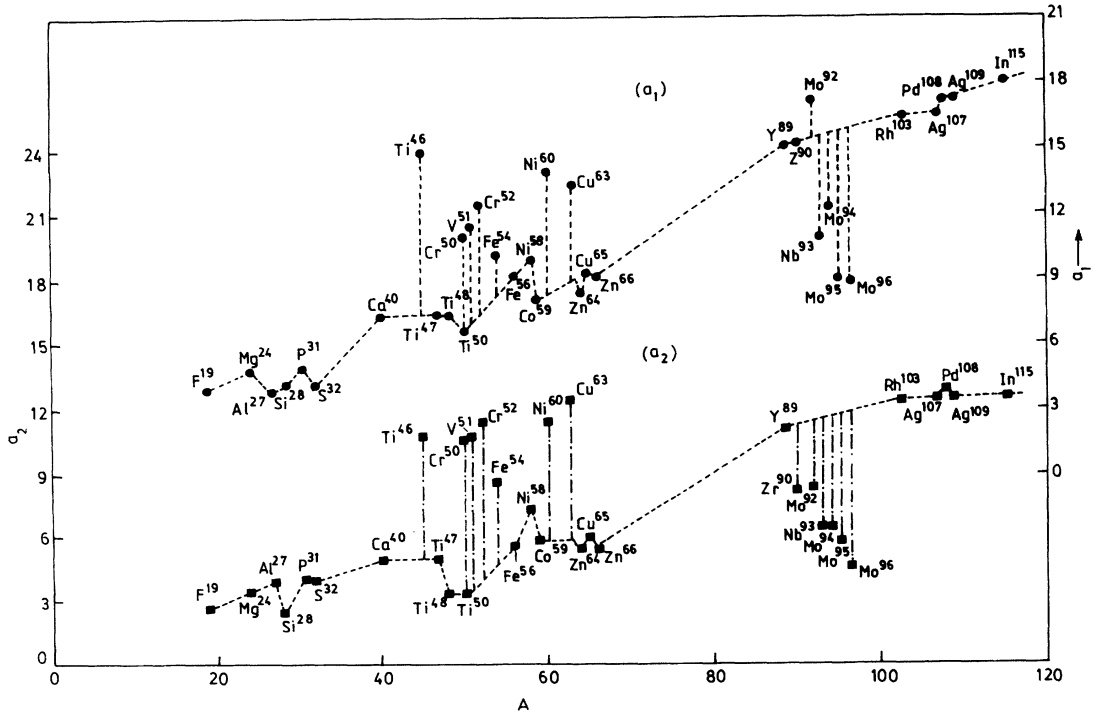

FIG. 5. The semiempirical values of level density parameters a_1 and a_2 (obtained from g's) as given in Table I, plotted against target mass number A. The upper curve for a_1 corresponds to the compound nucleus and lower one for a_2 corresponds to the residual nucleus.

$$R = \frac{D_{\text{exp}}}{D_{\text{Th-1}}} \tag{16}$$

is plotted as a function of the charge number of the target Z_T in Fig. 6(a). It is seen that, in general, $0.4 \leq R \leq 1.4$. We, however, may see that the comparison with experimental results obtained from energy integrated angular distributions (indicated by • with an error bar) give much better agreement, than those obtained form angle integrated energy spectra (indicated by △ with an error bar), because in the latter case the experimental results, Eq. 1(b), are dependent on the calculation of equilibrium spectrum from the Hauser-Feshbach model [38] which, in comparison, was found to overestimate the high-energy end of the spectrum compared to the Kalbach model.

C. Brown-Muirhead model [40]

In one of the very early attempts, Brown and Muirhead calculated the contribution of the direct reaction in a simple model [40]. They assumed the nucleus to consist of two independent Fermi gases of protons and neutrons and further assumed that the incident particle interacts individually with the bound nucleons of the target, within the limits of the Pauli exclusion principle. Then, one can write the cross section for the production of a proton with energy E, in the target nucleus as

$$\left(\frac{d\sigma}{dE}\right)_N = \sigma_1 \frac{\rho_p \left(\frac{d\sigma}{dE}\right)}{[\alpha X(P_1)]_{n,p}\rho_p + [\alpha X(P_1)]_{n,n}\rho_n}, \tag{17}$$

where $X(P_1)$ is the cross section for a collision of a neutron with momentum P_1, with a free nucleon [proton for (n,p) reactions and neutron for (n,n) reactions], α is a factor which reduces $X(P_1)$ inside the nucleus through the operation of Pauli exclusion principle, and ρ_p and ρ_n are the densities of protons and neutrons inside the nucleus. $d\sigma/dE$ is the cross section for the production of protons with energy E and σ_1 is the total absorption cross section of neutron at incident energy E_1.

Then one can write the expression for the direct ejection of a proton, with kinetic energy between E and $E + dE$, as

$$\left(\frac{d\sigma}{dE}\right)_{n,p} = \left(\frac{d\sigma}{dE}\right)_N \phi(E) \tag{18a}$$

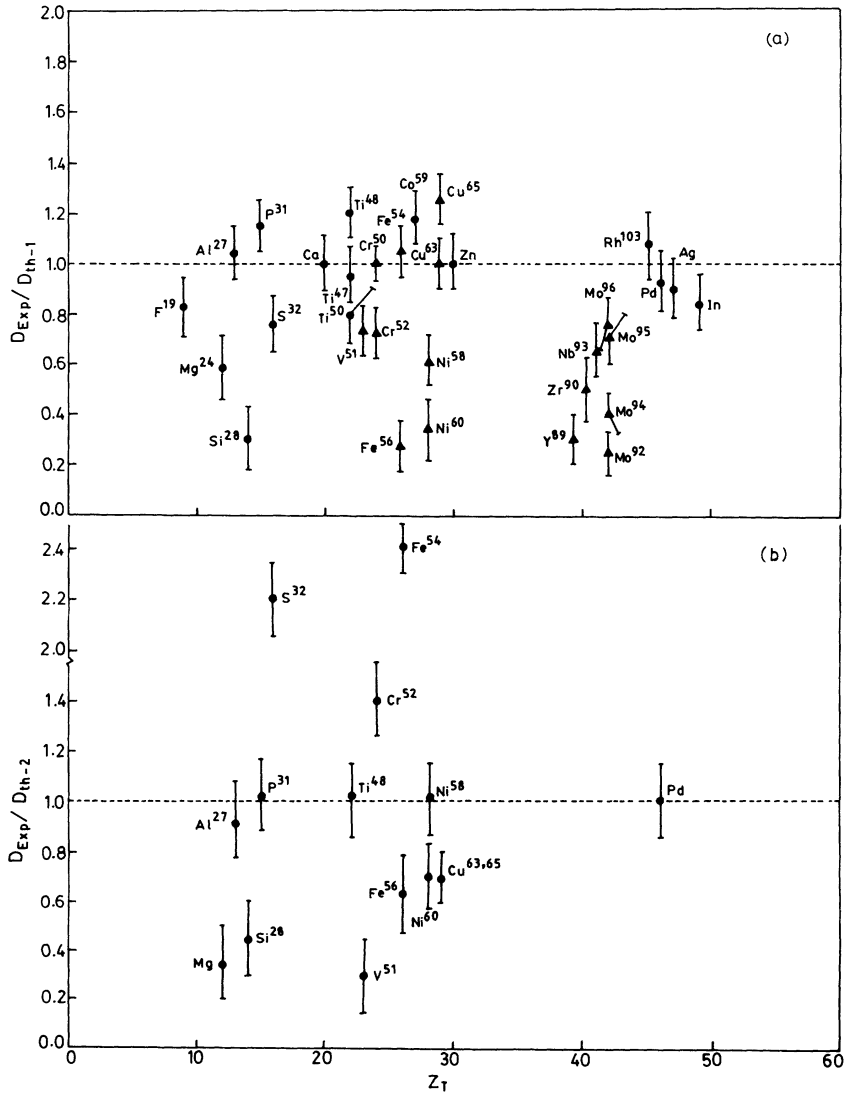

FIG. 6. (a) The ratio R between the $D_{(\text{Expt})}$ and $D_{\text{Th-1}}$ (Kalbach model) is plotted versus the target charge number Z_T. The points marked as • represent the comparison with data of energy integrated angular distributions, and ▲ represent the data of angle integrated energy spectra. (b) The ratio between $D_{(\text{Expt})}$ and $D_{\text{Th-2}}$ (Brown-Muirhead model) plotted as a function of target charge number Z_T.

and hence for a given $Q(n,p)$

$$\sigma_p(\text{dir}) = \int_0^{E_1+Q(n,p)} \left(\frac{d\sigma}{dE}\right)_{n,p} dE \ ; \qquad (18b)$$

then

$$D_{\text{Th-2}} = \frac{\sigma_p(\text{dir})}{\sigma_{\text{comp}} + \sigma_p(\text{dir})} \ , \qquad (19)$$

where $\phi(E)$ represents the probability of the escape and where σ_{comp} was taken from Ref. [51]. The values of $D_{\text{Th-2}}$ were calculated by Brown and Muirhead [40] directly for 14 MeV incident neutrons. We have produced in Table II results of the Brown-Muirhead model, i.e., $D_{\text{Th-2}}$ as given by them in their paper [40] to compare with the experimental results $D_{(\text{Expt})}$, as given in Fig. (1). In Fig. 6(b), we have plotted the ratio R between $D_{\text{Th-2}}$ and D_{Expt}. Evidently, the scatter of the points is much larger than a similar comparison with the Kalbach model, shown in Fig. 6(a). This is expected as the Brown-Muirhead model is a comparatively simple model, with no adjustable parameters, and also does not take into account the reflection of particles from the surface. However, we show the results to complete the comparison with reported theoretical data.

IV. SYSTEMATICS OF LEVEL DENSITY PARAMETERS

We have given in Table I and plotted in Fig. 5, the values of a_1 (related to g_c) and a_2 (related to g_R) versus the target mass number A. It may be pointed out that a_1 belongs to the compound nucleus ${}_Z(A+1)_{N+1}$ at an excitation energy of

$$U_1 = (14.8 + \text{B.E.}) \simeq 20 \text{ to } 25 \text{ MeV} \qquad (20)$$

and a_2 belongs to the residual nucleus ${}_{Z-1}A_{N+1}$ at an average excitation energy $\langle U_2 \rangle$ given by

$$\langle U_2 \rangle = \frac{14 \cdot 8 + Q}{2} \text{ MeV} \ , \qquad (21)$$

where Q is the Q value for n-p reaction for the target nucleus.

We now discuss the systematics which may be obtained from the values of a_1 and a_2.

(i) Both a_1 and a_2 increase with A. The individual values seem to vary around an average smooth curve, corresponding to $a_1 \simeq 0.16A$, and $a_2 \simeq 0.1A$. On the other hand, the dependence of average $a = (a_1 + a_2)/2$ on A in a similar manner comes out to be $a \simeq 0.12A$, if we exclude the region $45 \leq A \leq 63$, which contains abnormally high values of a_1 and a_2.

(ii) The values of a_1 are, in general, higher than the corresponding values of a_2 by a factor, which in some cases may be as large as 2, as shown in Table I.

(iii) There are two regions where the values of both a_1 and a_2 deviate abnormally from the general trend, i.e., (i) in the region of $45 \leq A \leq 63$, where the values are abnormally high, which we designate as "spikes" and (ii) in the region around $A \simeq 90$, where the values of both a_1 and a_2 are abnormally low, which we designate as "dips." We discuss below, these two regions separately. Both these regions correspond to nearly double magic numbers, i.e., the region of $45 \leq A \leq 63$ is around $N \simeq Z \simeq 28$, and the region of $A \simeq 90$ is around $Z \simeq 40$ and $N \simeq 50$.

(a) The region of spikes, i.e., $45 \leq A \leq 63$, involves nuclei like ${}_{24}\text{Cr}_{26}^{50}$, for which the compound nucleus as well as the residual nucleus have 27 neutrons—a hole in the closed shell of 28. In ${}_{23}\text{V}_{28}^{51}$, ${}_{24}\text{Cr}_{28}^{52}$, and ${}_{26}\text{Fe}_{28}^{54}$ both the compound and residual nuclei have 29 neutrons, i.e., a particle above the closed shell.

We have an interesting case of three nuclei in this region, i.e., ${}_{26}\text{Fe}_{28}^{54}$, ${}_{28}\text{Ni}_{32}^{60}$, and ${}_{29}\text{Cu}_{34}^{63}$, which have spikes, but other corresponding isotopes, i.e., ${}_{26}\text{Fe}_{30}^{56}$, ${}_{28}\text{Ni}_{30}^{58}$ and

TABLE I. Level density parameters a_1 and a_2 and the excitation energies U_1 and $\langle U_2 \rangle$ corresponding to compound and residual nuclei, respectively, and the parameters K and n of Rosenzweig power law as derived from Eqs. (21) and (22).

No.	Target	a_1	U_1 (MeV)	a_2	$\langle U_2 \rangle$ (MeV)	n	k
1	${}_9\text{F}^{19}$	4.1	21.4	2.5	5.4	1.3	0.8
2	${}_{12}\text{Mg}^{24}$	4.9	22.2	3.3	5.1	1.2	1.3
3	${}_{13}\text{Al}^{27}$	3.9	22.5	3.9	6.5	1.0	2.3
4	${}_{14}\text{Si}^{28}$	4.1	23.3	2.5	5.5	1.3	0.9
5	${}_{15}\text{P}^{31}$	4.6	22.7	4.1	7.0	1.0	2.4
6	${}_{16}\text{S}^{32}$	4.1	23.4	4.0	7.0	1.0	2.2
7	${}_{20}\text{Ca}^{40}$	7.4	23.2	4.9	7.9	1.3	1.3
8	${}_{22}\text{Ti}^{46a}$	15.2	23.7	11.2	6.6		
9	${}_{22}\text{Ti}^{47}$	7.4	25.7	4.9	7.3	1.3	1.3
10	${}_{22}\text{Ti}^{48}$	6.7	22.9	3.3	5.8	1.5	0.8
11	${}_{22}\text{Ti}^{50}$	6.7	21.2	3.3	4.3	1.4	1.0
12	${}_{23}\text{V}^{51a}$	11.4	22.1	10.7	6.6		
13	${}_{24}\text{Cr}^{50}$	10.7	24.1	10.7	7.3		
14	${}_{24}\text{Cr}^{52a}$	13.2	22.7	12.3	5.8		
15	${}_{26}\text{Fe}^{54a}$	9.9	24.1	9.0	7.5		
16	${}_{26}\text{Fe}^{56}$	9.0	22.4	4.9	6.0	1.4	1.1
17	${}_{27}\text{Co}^{59}$	8.2	22.3	4.9	7.0	1.4	1.1
18	${}_{28}\text{Ni}^{58}$	9.9	23.8	7.4	7.6	1.2	2.2
19	${}_{28}\text{Ni}^{60a}$	13.2	22.2	11.5	5.4		
20	${}_{29}\text{Cu}^{63a}$	13.2	22.7	12.4	7.7		
21	${}_{29}\text{Cu}^{65}$	9.0	21.4	6.6	6.8	1.2	2.2
22	${}_{30}\text{Zn}^{64}$	8.2	22.7	4.9	7.3	1.4	1.1
23	${}_{30}\text{Zn}^{66}$	9.0	21.8	4.9	6.5	1.4	1.3
24	${}_{39}\text{Y}^{89}$	14.8	21.7	10.7	7.0		
25	${}_{40}\text{Zr}^{90a}$	14.8	22.0	8.2	7.0		
26	${}_{41}\text{Nb}^{93a}$	10.7	22.0	6.6	7.8		
27	${}_{42}\text{Mo}^{92a}$	17.3	22.9	8.2	7.6		
28	${}_{42}\text{Mo}^{94a}$	12.4	22.2	6.6	7.3		
29	${}_{42}\text{Mo}^{95a}$	9.0	23.9	4.9	7.3		
30	${}_{42}\text{Mo}^{96a}$	8.8	21.6	4.8	6.2		
31	${}_{45}\text{Rh}^{103}$	16.5	21.7	12.4	7.4	1.2	1.4
32	${}_{46}\text{Pd}^{108}$	17.3	20.9	12.4	5.6	1.2	3.8
33	${}_{46}\text{Pd}^{106}$	18.1	21.3	11.4	6.1	1.3	2.4
34	${}_{47}\text{Ag}^{107}$	16.5	22.0	12.4	7.8	1.2	3.3
35	${}_{47}\text{Ag}^{109}$	17.3	31.6	12.4	7.6	1.3	2.9
36	${}_{49}\text{In}^{115}$	18.1	21.6	12.4	6.6	1.3	2.7

[a]Target nuclei which exhibit spikes and dips.

$_{29}Cu^{65}_{36}$ have normal values of a_1 and a_2 falling on the general curves. This shows the sensitivity of the single-particle level density to the details of pairing and some other effects.

In the literature [56–58[there is an indication of an unusual increase of a in this region, but it is not as prominent as that found in our analysis.

(b) The second "abnormal" region around $A \simeq 90$, which has dips in the values of a_1 and a_2, corresponds to nuclei $_{40}Zr^{90}_{50}$, $_{41}Nb^{93}_{52}$, $_{42}Mo^{92}_{50}$, $_{42}Mo^{94}_{52}$, $_{42}Mo^{95}_{53}$, and $_{42}Mo^{96}_{54}$. There is evidence of such a dip in the values of a in the literature [54–56] for $A \simeq 90$, obtained from thermal neutron resonance data. While our values of a_2 in this region are somewhat smaller than those given in the literature [56–59], our values of a_1 are higher, but the averages of a_1 and a_2 in this region are quite similar to the values of a in the literature.

(c) The semiempirical values of σ_{abs} as given in Table II show peaks for $_{26}Fe^{56}$, $_{26}Fe^{54}$, and $_{28}Ne^{60}$, and also for $_{40}Zr^{90}$ and $_{42}Mo^{95}$, showing the shell effects.

The nuclear structure level schemes as given in the *Nuclear Data Sheets* [60] for nuclei in the region of $45 \leq A \leq 63$, yield information about levels only up to 10–12 MeV excitations. Very high level density regions in many nuclei start from 4 to 5 MeV upwards, and, therefore, high level densities may be expected for lower excitation energies of 6–8 MeV excitation energy in this region of nuclei, corresponding to a high value of a_2. An interesting case [61] here is, that of $_{25}Mn^{54}$ and $_{25}Mn^{56}$, the residual nuclei obtained from (n,p) reaction on $_{26}Fe^{54}$ and $_{26}Fe^{56}$. The level density for $_{25}Mn^{54}$ as found in Ref. [61] is visibly higher than for $_{25}Mn^{56}$ at a 5–8 MeV excitation energy, as indicated in our measurements of a_2.

In a few cases [54–56] fits to higher excitation energies up to 20–23 MeV have been carried out for lighter nuclei, with a constant value of a, actually measured at $\simeq 8$ MeV excitation energy. Our analysis as given above, however, gives a direct evidence to the dependence of a on the excitation energy.

TABLE II. Relative preequilibrium contributions $D_{(Expt)}$, $D_{Th\text{-}1}$ (Kalbach model), and $D_{Th\text{-}2}$ (Brown-Muirhead model), and also the values of α_p (fraction of precompound decays). σ_{abs}, given in column four, corresponds to the best-fit normalized value of the absorption cross section [Eqs. (11) and (12)].

No.	Target nucleus	$D_{(Expt)}$	$D_{Th\text{-}1}$	σ_{abs} (mb)	$D_{Th\text{-}2}$	α_p	No.	Target nucleus	$D_{(Expt)}$	$D_{Th\text{-}1}$	σ_{abs} (mb)	$D_{Th\text{-}2}$	α_p
1	$_9F^{19}$	0.14 (17,25)	0.17	971.8 × 0.36	0.62	0.70	18	$_{28}Ni^{58}$	0.12 (32)	0.18	1606.9 × 5.5	0.11	0.09
2	$_{12}Mg^{24}$	0.08 (18)	0.14	1083 × 3.8	0.24	0.35	19	$_{28}Ni^{60}$	0.15 (32)	0.46	1624 × 2.5	0.21	0.06
853	$_{13}Al^{27}$	0.54 (18)	0.5	1134.3 × 1.0	0.57	0.85	20	$_{29}Cu^{63}$	0.31 (32)	0.28	1659 × 1.3	0.45	0.06
4	$_{14}Si^{28}$	0.08 (18)	0.22	1158.6 × 3.3 7	0.18	0.32	21	$_{29}Cu^{65}$	0.5 (32)	0.4	1676 × 0.3	0.75	0.15
5	$_{15}P^{31}$	0.52 (18)	0.45	1206 × 8.3	0.50	0.90	22	$_{30}Zn$	0.4 (18)	0.41	1676 × 0.3	0.13	0.1
6	$_{16}S^{32}$	0.45 (18)	0.6	1229 × 1.0	0.20	0.85	23	$_{39}Y^{89}$	0.14 (32)	0.40	1948 × 2.0		0.005
7	$_{20}Ca^{40}$	0.17 (20)	0.18	1359 × 2.2		0.15	24	$_{40}Zr^{90}$	0.20 (32)	0.37	1963 × 4.0	0.46	0.008
8	$_{22}Ti^{46}$	0.05 (34)	0.05	1439 × 1.1		0.012	25	$_{41}Nb^{93}$	0.30 (31)	0.49	1992 × 0.25		0.01
9	$_{22}Ti^{47}$	0.18 (34)	0.19	1449.3 × 1.1		0.03	26	$_{42}Mo^{92}$	0.02 (33)	0.08	2000 × 0.5		0.001
10	$_{22}Ti^{48}$	0.24 (34)	0.20	1459.1 × 1.5	0.23	0.09	27	$_{42}Mo^{94}$	0.21 (33)	0.59	2007 × 1.7		0.006
11	$_{22}Ti^{50}$	0.42 (33)	0.58	1478.1 × 2.0		0.42	28	$_{42}Mo^{95}$	0.41 (33)	0.57	2015 × 4.5		0.01
12	$_{23}V^{51}$	0.25 (31)	0.34	1497 × 2.0	0.61	0.11	29	$_{42}Mo^{96}$	0.45 (33)	0.60	2022 × 1.8		0.008
13	$_{24}Cr^{50}$	0.18 (32)	0.18	1497 × 2.0		0.05	30	$_{45}Rh^{103}$	0.65 (9)	0.6	2094 × 0.42		0.01
14	$_{24}Cr^{52}$	0.35 (32)	0.48	1516 × 2.0	0.25	0.02	31	$_{46}Pd$	0.70 (9)	0.75	2137 × 4.0	0.7	0.003
15	$_{26}Fe^{54}$	0.22 (32)	0.21	1552.9 × 4.5	0.09	0.065	32	$_{47}Ag$	0.50 (37)	0.56	2137 × 4.0		0.005
16	$_{26}Fe^{56}$	0.14 (32)	0.33	1571 × 4.5	0.27	0.045	33	$_{49}In^{115}$	0.50 (37)	0.6	2206 × 3.0		0.002
17	$_{27}Co^{59}$	0.46 (18)	0.39	1606.9 × 0.3		0.22							

V. EXCITATION ENERGY DEPENDENCE OF SINGLE-PARTICLE LEVEL DENSITIES

Our analysis seems to be one of the few cases [62] providing direct experimental information about single-particle level densities at higher excitation energies of 20–25 MeV for so many nuclei. However, the dependence of the values of g's on excitation energies has been discussed, theoretically earlier by some workers [47,58], especially by Rosenzweig [47], who assumed a general positive power law, so that $g_n(\epsilon)$ [expressed as $\rho(\epsilon)$ in Eq. (9) in his first paper [47], could be expressed as

$$g_n(\epsilon) = k^n \epsilon^{n-1} , \tag{22}$$

where k is a constant and ϵ is the excitation energy of the levels.

In the absence of any extensive experimental data the dependence of $g_n(\epsilon)$ on ϵ was estimated by Rosenzweig [47] to correspond to $n = 1.6$ assuming that the binding energy ϵ' of the last nucleon is about 8 MeV and the invididual particle levels are regarded as eigenvalues of a suitable potential well depth V, so that $V - \epsilon' \simeq 40$ MeV.

With the present analysis, we now have the semiempirical values of a_1 and a_2 at two excitation energies U_1 and $\langle U_2 \rangle$ for a large number of cases. It should be, therefore, possible to obtain a semiempirical value of n from the fact that

$$\left(\frac{a_1}{a_2}\right) = \left(\frac{U_1}{\langle U_2 \rangle}\right)^{n-1} . \tag{23}$$

The value of $\langle U_2 \rangle$ used in this manner can be taken only as approximate. We are further assuming that n is a constant, independent of ϵ: for a given nucleus, though, it could have variations for different nuclei. The deviation of n from 1 indicates the significance of nondegeneracy in individual particle levels, at the higher excitation energy, giving rise to nonequidistant single-particle energy levels. We have given in Table I the values of n for each nucleus, obtained from Eq. (22), and have plotted n as a function of A in Fig. 7(a). As the values of a_1 and U_1 and a_2 and $\langle U_2 \rangle$, against each target nucleus given in Table I belong to different nuclei, we obtained from the interpolation from Fig. 5 the proper values of a_2 so that it belongs to the same nucleus as corresponds to a_1. For this purpose, only the regions of A corresponding to a smooth variation of a_2 were used, i.e., in the ranges of $19 \leq A \leq 50$ and $100 \leq A \leq 115$. The regions of A having spikes and dips could not be used for this purpose.

A few points emerge.

(i) For some light nuclei, i.e., ^{27}Al, ^{31}P, and ^{32}S we have the value of $n \simeq 1.0$, corresponding to the fact that the nondegeneracy is not significant for these nuclei up to 20–23 MeV.

(ii) All other cases have $1.2 \leq n \leq 1.5$, but do not show any systematic dependence on A. The value of n is somewhat smaller than the value of $n \simeq 1.6$ as given by Rosenzweig [47].

(iii) The values of k for these cases seem to vary between 0.8 and 3.8 and are generally nucleus specific; they also show a trend of a slow increase of k with A.

(iv) The regions of $40 \leq A \leq 63$, and $89 \leq A \leq 96$ are regions of spikes and dips, and though it is not possible to calculate the values of n and k through interpolation, it is interesting, however, to note that in both these regions, shell effects persist in a_1 as in a_2, suggesting $n \gtrsim 1$.

VI. SUMMARY AND CONCLUSION

The analyzed results of preequilibrium contributions, i.e., D's (Fig. 1), from the global data of the energy integrated angular distribution and angle integrated energy spectra of protons from (n,p) reactions at 14 MeV nominal incident energy have been compared in detail with the Blann-Griffin [41], Kalbach [42–46], and Brown-Muirhead [40] models and the Rosenzweig [47] power law.

Application of the Blann-Griffin model to the data brings out an interesting feature that while for $A \simeq 72$ fraction of decays into continuum from precompound channel (α_p) approaches zero ($\alpha_p \ll 0.1$): it steadily increases for lighter nuclei until for very light nuclei, it approaches 1 (Fig. 3). The model assumes only a small and constant value of α_p. This shows that for light nuclei, perhaps the surface plays a bigger role in preequilibrium emission, which the model has not taken into account adequately.

The comparison of the data, with the Feshbach-Kerman-Koonin [42] and Kalbach [42–46] models, has, however, given much better insight into the reaction mechanism. The theoretical fits to the experimental data—both of proton energy spectra and angular distributions (Fig. 4)—have yielded values of a_1 and a_2, over the region of $A = 19$–115, showing a smooth increase in the values of a_1 and a_2 with A, except in the region of $A \simeq 90$, where there are dips, and in the region of $45 \leq A \leq 63$, where there are spikes in the values of a_1 and a_2 (Fig. 5) showing shell effects.

The values of precompound contributions D(Expt) (Fig.1), when compared with the Kalbach [42–46] and Brown-Muirhead models [40], show that the Kalbach model with the adjusted parameters fits the experimental data better (Fig. 6) and also explains to a large extent the trend of increase in D(Expt) with A (Fig. 2). The comparison with Rosenzweig's power law [47], for excitation energy dependence of g's, shows that the dependence is nuclear specific. The value of n in the regions of smooth behavior of the curve is $1.20 \leq n \leq 1.5$ and k varies from 0.8 to 3.8 and increases slowly with A (Fig. 7), except for light nuclei, i.e., ^{27}Al, ^{31}P, and ^{32}S, where $n \simeq 1$.

In brief, we may conclude, from the above analysis, that an increase in the value of the single-particle level densities g with excitation energy, for the same A is clearly indicated, and that the Fermi gas model, using equidistant single-particle energy levels may be taken as

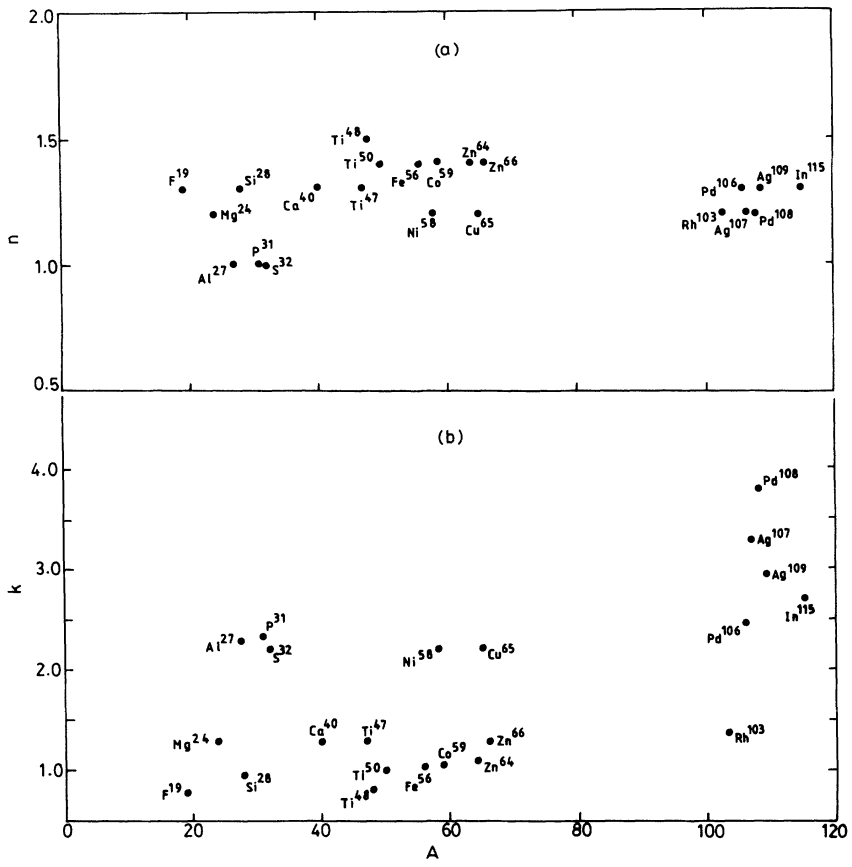

FIG. 7. (a) The values of parameter n of the Rosenzweig power law Eq. (22) for different nuclei. (b) The values of parameter k [Eq. (21)] of the Rosenzweig power law for different nuclei.

an approximation only. To extract the variation of the single-particle level density, with excitation energy, it is necessary to analyze the energy spectra or angular distributions, with varying projectile energy for a given target. If the change in the level density parameter with excitation energy is found to be significant, then the currently used expressions for level densities, both total and partial, will have to be appropriately modified.

[1] Murrey D. Goldberg, Victoria M. May, and John R. Stehn, National Neutron Cross Section Center, Brookhaven National Lab. Upton, N.Y., Report No. BNL-400, V.1, 2 (1962:1970) (unpublished).
[2] Sol Pearlstein, L. Lesca, and J. J. Schmidt, International Atomic Energy Agency, Vienna, Report No. CINDA 76/77, v. 1,2 (1976) (unpublished).
[3] L. Colli, U. Facchini, I. Iori, M. G. Marcazzan, and A. M. Sona, Nuovo Cimento **13**, 730 (1959): L. Colli, F. Cvelbar, S. Micheletti, and M. Pignanalli, *ibid.* **13**, 868 (1959).
[4] L. Colli, F. Cvelbar, S. Micheletti, and M. Pignanelli, Nuovo Cimento **14**, 1120 (1959).
[5] L. Colli, I. Iori, S. Micheletti, and M. Pignanelli, Nuovo Cimento **21**, 966 (1961).
[6] D. L. Allan, Nucl. Phys. **24**, 274 (1961).
[7] U. Facchini, I. Iori, and E. Menichella, Nuovo Cimento **16**, 1109 (1960).
[8] E. Ebra, U. Facchini, and E. Saetta Menichella, Nuovo Cimento **22**, 1248 (1961).
[9] V. V. Verbinsky, T. Huslimann, W. E. Stephan, and E. J. Winbold, Phys. Rev. **108**, 779 (1957).
[10] S. H. Ahn, J. R. Hearst, J. H. Roberts, and E. N. Sirait, Phys. Rev. **119**, 1667 (1960).
[11] L. Colli, I. Iori, C. Marcazzan, F. Mezari, A. M. Sona, and P. G. Soha, Nuovo Cimento **17**, 634 (1960).
[12] W. Jack and A. Ward, Proc. Phy. Soc. **75**, 526 (1960); **75**, 833 (1960).
[13] H. P. Eubank, R. A. Peck, and M. R. Zatzik, Nucl. Phys. **10**, 418 (1959).
[14] R. A. Peck, H. P. Eubank, and R. M. Howard, Nuovo Cimento **14**, 397 (1959).
[15] A. H. Armstrong and L. Rosen, Nucl. Phys. **19**, 40 (1960).
[16] R. A. Peck, Jr., Phys. Rev. **123**, 1738 (1961).
[17] J. Furkiewiez, Phys. Rev. **127**, 570 (1962).
[18] F. L. Hassler and R. A. Peck, Jr., Phys. Rev. **125**, 1011 (1962).
[19] L. Colli, M. Maggialajo, F. Marcelza, F. Merzari, and P. G. Sona, Nuovo Cimento **29**, 983 (1963).
[20] R. K. Mohindra and H. S. Hans, Nucl. Phys. **44**, 597 (1963).
[21] W. R. Dixon, Nucl. Phys. **42**, 27 (1963).
[22] H. S. Hans and R. K. Mohindra, Nucl. Phys. **43**, 59 473 (1963).
[23] J. C. Robetson, Nucl. Phys. **49**, 306 (1963).
[24] H. Morgenstern, D. Hilscher, and J. Scheer, Nucl. Phys. **83**, 369 (1966).

[25] D. Rendic, B. Antolkovie, G. Pair, M. Furk, and P. Tomas Nucl. Phys. **A117**, 113 (1968).
[26] A. Kartase, T. Akiyostu, M. Sonoda, and Masso Seki, Nucl. Phys. **A111**, 184 (1968).
[27] K. A. Alvar, Nucl. Phys. **A195**, 289 (1972).
[28] A. Salinovo, G. N. Lovichikova, G. V. Kotelmikova, A. M. Turfomov, and N. I. Festisor, Yad. Fiz. **12**, 1132 (1977) [Sov. J. Nucl. Phys. **12**, 620 (1977)].
[29] S. M. Grimes and J. D. Anderson, J. W. Mcclure, B. A. Poll, and C. Wong, Phys. Rev. C **10**, 2373 (1974).
[30] S. M. Grimes, R. C. Haight, and J. D. Anderson, Nucl. Sci. Eng. **62**, 187 (1977).
[31] S. M. Grimes, R. C. Haight, and J. D. Anderson, Phys. Rev. C **17**, 508 (1978).
[32] S. M. Grimes, R. C. Haight, K. R. Alvar, H. H. Barschall, and R. R. Borchers, Phys. Rev. C **19**, 2127 (1979).
[33] R. C. Haight, S. M. Grimes, P. G. Johnson, and H. H. Barschall, Phys. Rev. C **23**, 700 (1981).
[34] I. Rebamsky and S. Gmuca, J. Phys. **9**, 1537 (1983).
[35] R. Bonnetti, L. Colli Milazzo, and M. Melanotte, Phys. Rev. C **27**, 1003 (1983).
[36] P. M. Field, R. Bonnetti, and P. E. Hodgson, J. Phys. G **12**, 93 (1986).
[37] R. Fischer, M. Uhl, and H. Vonach, Phys. Rev. C **37**, 578 (1988).
[38] H. Feshbach, Rev. Mod. Phys. **46**, 1 (1974).
[39] M. Blann, Ann. Rev. Nucl. Sci. **25**, 123 (1975).
[40] G. Brown and M. Muirhead, Philos. Mag. **2**, 473, 785 (1957).
[41] J. J. Griffin, Phys. Rev. Lett. **17**, 478 (1966); M. Blann, *ibid.* **21**, 1357 (1968).
[42] H. Feshbach, A. Kerman, and S. Koonin, Ann Phys. (N.Y.) **125**, 429 (1980).
[43] C. Kalbach, Phys. Rev. C **23**, 124 (1981): **24**, 819 (1981).
[44] C. Kalbach and F. M. Mann, Phys. Rev. C **23**, 112 (1981); **25**, 3197 (1982).
[45] C. Kalbach, Z. Phys. A **283**, 401 (1977).
[46] C. Kalbach, PRECO-D2 program for calculating the preequilibrium and direct reaction double-differential cross sectional, Los Alamos National Lab. LA 10248-MS, 1985.
[47] N. Rosenzweig, Phys. Rev. **105**, 950 (1957); **108**, 817 (1957).
[48] J. M. Blatt and V. F. Weisskopf, *Theoretical Nuclear Physics* (Wiley, New York, 1952), p. 352.
[49] V. V. Verbinski and W. R. Burrus, Phys. Rev. **1177**, 1671 (1969).
[50] P. K. Sarkar, T. Bandopadhye, G. Muthukrishnan, and Sudip Ghosh, Phys. Rev. C **43**, 1855 (1991).
[51] V. F. Weisskopf and D. H. Ewing, Phys. Rev. **57**, 472 (1940).
[52] A. Chatterjee, K. H. N. Murty, and S. K. Gupta, Pramana **16**, 391 (1981).
[53] A. Gilbert and A. G. W. Cameron, Can. J. Phys. **43**, 1446 (1965).
[54] H. Baba, Nucl. Phys. **A159**, 625 (1970).
[55] C. C. Lu, L. C. Vaz, and J. R. Huizenga, Nucl. Phys. **A190**, 229 (1972).
[56] W. Dilg, W. Schantl, H. Vonach, and M. Uhl, Nucl. Phys. **A217**, 269 (1974).
[57] T. Von Egidy, H. H. Schmidt, and A. H. Behkami, Nucl. Phys. **A481**, 189 (1988).
[58] J. R. Huizenga and L. G. Moretto, Annu. Rev. Nucl. Sci. **22**, 427 (1972).
[59] L. G. Moretto, Nucl. Phys. **A182**, 641 (1972).
[60] *Nuclear Data Sheets*, edited by M. J. Martin and J. K. Tuli (Academic, New York, 1983–1992), Vols. 38–67.
[61] Wang Gongging *et al.*, *Nuclear Data Sheets* (Academic, New York, 1987), Vol. 50, p. 255; Huojunde *et al.*, *ibid.*, Vol. 51, p. 1.
[62] J. M. Akkermans, H. G. Gruppelaar, and G. Reffo, Phys. Rev. C **22**, 73 (1980).